Appendix A

SPECTROELLIPSOMETRIC ANALYSIS OF NIO LAYERS GROWN ON NI

A.1. Experiment

A phase modulated spectroscopic ellipsometer comprises, on its incident light arm, a light source, a polariser and a modulator, while the reflected light passes through an analyser and monochromator before detection by a photodiode [1,2]. The experiments reported here were carried out using light from a Xe arc lamp (energy range: 1.5 eV to 5 eV). The photoelastic modulator (PEM) consists of a rectangular fused silica block cemented onto a piezoelectric quartz crystal oscillating at a frequency of $w = 50$ kHz [3]. The oscillating crystal induces an uniaxial sinusoidal standing strain wave in the silica block, thereby establishing a time varying birefringence. The light beam transmitted by the quartz crystal is characterised by a periodic relative phase shift (δt) between its orthogonal amplitude components:

$$dt = I \cdot \sin(wt), \qquad \text{(A.1)}$$

with a modulation amplitude (I) which depends on the excitation voltage applied to the piezoelectric crystal and the light wavelength. Since the optical properties of the PEM are temperature dependent a constant working temperature of 30°C ± 0.01°C is maintained by thermoelectrical temperature regulation. Analyser and polariser materials are quartz glans with an extinction coefficient better than 10^{-4}. Polariser, modulator and analyser are mounted on rotating plates with a rotation accuracy better than 0.05°. Optical coupling between all components is made via UV-grade fiber optical cables of length: 2 m with a core diameter of 1 mm.

Space constraints prevent a detailed derivation of the calculus using Müller matrices and Stokes parameters which underlies the polarisation modulated measurement of the ellipsometric angles y and D. These angles are defined *via* the complex reflectance ratio

$$r = r_p / r_s = \tan(y) \cdot \exp(iD) \qquad \text{(A.2)}$$

where the subscripts p and s refer to the plane wave electric field components, respectively, parallel and perpendicular to the incidence plane. The orientations of polariser, modulator and and analyser will be referred to as P, M, and A, respectively. The important result of the Stokes/Müller calculus is that the intensity of the beam takes the general form [4]

$$I(t) = I_0 + I_s \cdot \sin d(t) + I_c \cdot \cos d(t) \qquad \text{(A.3a)}$$

where

$$I_0 = \frac{\left|r_p^2 + r_s^2\right|}{4} \cdot \begin{pmatrix} 1 + \cos(2A) \cdot \cos(2M) \cdot \cos(2(M-P)) - \ldots \\ \ldots - (\cos(2A) + \cos(2M) \cdot \cos(2(M-P)) \cdot \cos(2y)) \end{pmatrix} \quad \text{(A.3b)}$$

$$I_s = \frac{\left|r_p^2 + r_s^2\right|}{4} \cdot \left(-\sin(M-P) \cdot \sin(2A) \cdot \sin(2y) \cdot \sin(\Delta)\right) \quad \text{(A.3c)}$$

$$I_c = \frac{\left|r_p^2 + r_s^2\right|}{4} \cdot \left(-\sin(2(M-P)) \cdot \begin{pmatrix} \sin(2M) \cdot \left(\cos(2y) - \cos(2A)\right) + \ldots \\ \ldots + \cos(2M) \cdot \sin(2A) \cdot \sin(2y) \cdot \cos(\Delta) \end{pmatrix} \right) \quad \text{(A.3d)}$$

The Fourier expansions of the sine and cosine of the modulation amplitude *d(t)* are [1]

$$\sin d(t) = 2 \sum_{m=0}^{\infty} J_{2m+1}(A) \cdot \sin\left((2m+1) \cdot wt\right) \quad \text{(A.4a)}$$

$$\cos d(t) = J_0(A) + 2 \sum_{m=1}^{\infty} J_{2m}(A) \cdot \cos(2m \cdot wt) \quad \text{(A.4b)}$$

where $J_n(A)$ are Bessel functions of order n and argument A. The ratios of the fundamental (R_w) and the second harmonic (R_{2w}) component to dc component of the detected beam intensity allow the determination of y and D according to

$$R_w = \frac{2 \cdot J_1(A) \cdot I_s}{I_0 + J_0(A) \cdot I_c} \quad \text{(A.5a)}$$

$$R_{2w} = \frac{2 \cdot J_2(A) \cdot I_c}{I_0 + J_0(A) \cdot I_c} \quad \text{(A.5b)}$$

These expressions can be simplified by adjusting the modulation amplitude I so that $J_0(A) = 0$ (fulfilled for A = 2.405 rad). This allows to define two sets of convenient measurement configurations for which the expressions for R_w and R_{2w} are particularly simple; modulator and polariser are held at a relative orientation of M-P = 45° resulting in the two convenient combinations for modulator and analyzer orientations:

	CONFIGURATION 1	CONFIGURATION 2
M	-45°	0°
A	-45°	-45°

For configuration 1, y and D are given by

$$R_w = 2 \cdot J_1(A) \cdot \sin(2y) \cdot \sin(\Delta) \qquad \text{(A.6a)}$$

$$R_{2w} = 2 \cdot J_2(A) \cdot \cos(2y) \qquad \text{(A.6b)}$$

and for configuration 2 by

$$R_w = 2 \cdot J_1(A) \cdot \sin(2y) \cdot \sin(\Delta) \qquad \text{(A.7a)}$$

$$R_{2w} = 2 \cdot J_2(A) \cdot \sin(2y) \cdot \cos(\Delta) \qquad \text{(A.7b)}$$

Recording the first and second Fourier components of the reflected and monochromatised light beam thereby allows the determination of the ellipsometric angles and the complex reflectance ratio. On-line Fourier analysis can be performed by use of a lock-in amplifier [5] or, as in the present study, digitally in the process computer [1]. The instrumental error in y and D is typically less than 0.5°. Systematic errors are mainly introduced by misalignment of the sample and/or unwanted depolarisation effects [6].

A.2. Data Analysis

For a given angle of light incidence f_0 at an interface between air and a semi-infinite medium, the measured complex ratio r of the Fresnel reflection coefficients determines a complex pseudodielectric function $\tilde{e}$

$$\tilde{e} = \tilde{e}_1 + i \cdot \tilde{e}_2 = \sin^2 f_0 \cdot \left(1 + \tan^2 f_0 \cdot \frac{(1-r)^2}{(1-r)^2} \right). \qquad \text{(A.8)}$$

$\tilde{e}$ is related to the complex pseudo-refractive index $\tilde{n}$, the pseudo-refractive index n and the pseudo-extinction coefficient k by

$$\tilde{e} = \tilde{n}^2 = (n^2 - k^2) + 2ink \qquad \text{(A.9)}$$

The analysis of the pseudodielectric function of a 2-layer stratified medium is made possible by the fact that the composite Fresnel reflection coefficient (r_s or r_p) is related to the reflection coefficients of the layers by [7]

$$r = \frac{r_l + r \cdot \exp(-2i \cdot b_l)}{1 + r_l \cdot r \cdot \exp(-2i \cdot b_l)}, \qquad \text{(A.10a)}$$

where r and r_l denote the reflectance of the substrate and the overlayer surface, respectively. b_l is calculated according to

$$b_l = \frac{2p \cdot d_l}{l} \cdot \tilde{n}_l \cdot \cos(f_l), \qquad \text{(A.10b)}$$

with the thickness d_l of the overlayer film, and l the wavelength of the incident light. The complex angle of incidence f_l for the overlayer material is calculated according to Snell's law

$$\sin(f_l) = \frac{\tilde{n}_0}{\tilde{n}_l} \cdot \sin(f_0), \qquad \text{(A.10c)}$$

with the complex refractive indices $\tilde{n}_0$ and $\tilde{n}_l$ of the ambient and the overlayer material, and the complex angle of incidence f_0 with respect to the surface normal of the interface between sample and ambient.

If the dielectric functions of the sample components are known then an unknown overlayer thickness can be determined from the measured pseudodielectric function by using equations (A.8)-(A.10). For the present study, the dielectric function of the Ni substrate was known to high accuracy over a wide range of energies [8]. The dielectric function of NiO, not available from the literature, was simulated using a damped single Lorentz oscillator model. The parameters of the model were determined simultaneously with the overlayer thickness and void concentration (see below) by a c^2-fit to the pseudodielectric function. This modelling approach has previously been applied successfully to the thickness analysis of insulating overlayers of other diatomic materials, including MgO, ZnS and SiO_2 [6,7,9-11]. The choice of the simple single oscillator model for the diatomic ionic crystal is justified on the grounds that most of the interactions between electromagnetic waves and ionic crystals in the spectral range between 1 eV and 5 eV is due to the excitation of lattice vibrations of the optical branch [12].

The derivation of the dispersion relation for the dielectric constant of an ionic, diatomic lattice within the undamped single oscillator model can be found in most modern solid-state physics textbooks (e.g., in ref. [12,13], but see also refs. [14,15]). Briefly, the model is based on the assumption that the crystal lattice has cubic symmetry, with two atoms per primitive basis. Each atom only interacts with unlike nearest neighbours and the force constants between unlike neighbours are identical throughout the crystal. The resulting dispersion formula reads [12-15]

$$e(w) = e_\infty + \frac{e_0 - e_\infty}{1 - \left(w/w_0\right)^2}, \qquad \text{(A.11)}$$

where w_0 is the infrared dispersion frequency at which the refractive index and the dielectric constant become infinitely large (*i.e.*, the single oscillator lattice becomes

perfectly light reflecting), while e_0 and e_∞ are the static and high-frequency (with w much larger than w_0) dielectric constants, respectively. This simple single oscillator model for the diatomic ionic crystal predicts total reflection when the light frequency w approaches w_0. In real crystals, total reflection does not occur because some light energy is always absorbed and dissipated by the lattice [14]. A popular *ad hoc* extension of the undamped model which takes account of energy dissipation involves the introduction of a simple damping term into the equation of motion underlying the single oscillator approximation [14]. The resulting dispersion relation is of similar form as in the undamped case, but the dielectric function becomes complex [13,14]:

$$e(w) = e_\infty + \frac{e_0 - e_\infty}{1 - \left(w/w_0\right)^2 - ig \cdot w/w_0^2}. \qquad \text{(A.12)}$$

The damping term in the equation of motion represents a force always opposed to the atomic motion, resulting in a characteristic damping constant g which has the dimensions of frequency. The damped oscillator model reduces to the undamped case for $g = 0$. It is important to bear in mind that the introduction of g represents a purely phenomenological extension to the simple theory, intended to account for the fact that the real crystal lattice actually absorbs light due to coupling between transverse and longitudinal modes of lattice vibrations. A large fitted value for g can therefore be indicative of any absorption mechanism, which is not necessarily vibrational coupling.

Equation (A.12) allows identification of the real and imaginary parts of the dielectric function defined in equations (A.8) and (A.9) according to [14]

$$e_1 = n^2 - k^2 = e_\infty + \frac{(e_0 - e_\infty)\cdot\left(1-(w/w_0)^2\right)}{\left(1-(w/w_0)^2\right)^2 + (w/w_0)^2\cdot(g/w_0)^2} \qquad \text{(A.13a)}$$

$$e_2 = 2nk = \frac{(e_0 - e_\infty)\cdot(g/w_0)\cdot(w/w_0)}{\left(1-(w/w_0)^2\right)^2 + (w/w_0)^2\cdot(g/w_0)^2}. \qquad \text{(A.13b)}$$

Note that the dispersion relation (A.12) demands that n and k have the same sign since $e_0 > e_\infty$. The sign of $\tilde{n}$ in equation (A.9) is conventionally chosen such that both n and k are positive [14].

Porosity in the NiO films was accounted for by applying the Maxwell-Garnett (MG) effective medium approximation [16,17] to the dielectric function of the overlayer. The MG theory was originally conceived to describe optical absorption in small metal particles, which the theory treats as polarisable spherical inclusions in an ambient host medium. The theory thereby accounts for the modifications of an

applied electrical field by the dipole field of these small particles. For the MG theory to be valid, the particles must be sufficiently large so that the macroscopic Maxwell equations can be applied, but still smaller than the attenuation length (which, approximately, equals the wavelength) of the absorbed light.

The derivation of the MG expression starts from the familiar [12] Clausius-Mosotti equation (given in cgs units)

$$\frac{e(w)-1}{e(w)+2}=\frac{4}{3}\cdot p\cdot n\cdot a(w), \qquad \text{(A.14)}$$

which expresses the relationship between the dielectric constant $e(w)$ of the effective medium, the volume density of the medium n, and the polarisability $a(w)$ of the metal particles [18]. This equation assumes that the metal particles are dispersed in *vacuum*, rather than in a *polarisable insulator* characterised by the dielectric constant $e_i(w)$. Taking account of this difference, the more generalised Clausius-Mosotti equation

$$\frac{e(w)-e_i(w)}{e(w)+2\cdot e_i(w)}=\frac{4\cdot p\cdot n\cdot a(w)}{3\cdot e_i(w)} \qquad \text{(A.15)}$$

is obtained [18]. Replacing for $a(w)$ the expression for the polarisability of an isolated metal sphere immersed in a medium of dielectric constant $e_i(w)$ [19] yields the original MG result

$$\frac{e(w)-e_i(w)}{e(w)+2\cdot e_i(w)}=(1-x)\cdot\frac{e_m(w)-e_i(w)}{e_m(w)+2\cdot e_i(w)}, \qquad \text{(A.16)}$$

where $e_m(w)$ is the dielectric constant of the metal and x is the volume fraction of the insulator. As shown by Galeener [20,21] and Cohen *et al.* [18], this result can be further generalised for any ellipsoidal shape of the metal particles by introducing a characteristic depolarisation factor L:

$$\frac{e(w)-e_i(w)}{e(w)+2\cdot e_i(w)}=\frac{1}{3}\cdot(1-x)\cdot\frac{e_m(w)-e_i(w)}{L\cdot e_m(w)+(1-L)\cdot e_i(w)}. \qquad \text{(A.17)}$$

In the limit of $L = 0$ the particles are flat platelets, and in the limit of $L = 1$ they are infinitely long, 'needle-like' crystallites. It is now a straightforward matter to show that the original MG result for spherical metal particles corresponds to $L = 1/3$.

It has long been recognised by optical spectroscopists that the MG concept is also applicable to the calculation of the dielectric properties of a heterogeneous medium, Many workers have applied the MG effective medium theory to the analysis of ellipsometric data of porous and/or rough films [7,22-24]. In this case, the voids in

the film take on the rôle of the metallic particles and are treated as inclusions in the host film material.

The MG approach is somewhat open to critique, on the grounds that the effective dielectric function is not invariant under the exchange of the rôles of host and inclusion [22]. This physical inconsistency can be resolved by using a modification introduced by Brüggeman [25] who pointed out that self-consistency can be achieved by letting the effective medium itself act as the host medium ($e(w) = e_i(w)$). The Brüggeman approach has recently been adopted more widely (see, e.g., [6,7,9,11,23,26-29]) because it is also less limited by the constraints imposed by the ellipsoidal shape of the inclusions assumed in the MG model [23,24]. However, the results obtained by the Brüggeman approach do usually agree quite reasonably with those obtained with a MG treatment, *if the voids in the inhomogeneous medium are treated as the inclusions* [22]. In line with this, it was found that the volume fraction of voids determined by a Brüggeman analysis of the NiO overlayers analysed in the present work was, for most samples, only lower by approximately 15% than for the MG analysis, while the fit quality did not vary significantly between the models (see fig. A.2 below). The fitted single oscillator dielectric constants of the host material were consistently somewhat lower in the Brüggeman than in the MG model. This observation is readily understood because the MG approach weights the effective dielectric function more towards the contribution of the host material [18,22,30,31]. The difference between the MG and Brüggeman results has been taken account of by increasing the error margin of the determined NiO overlayer thicknesses (see table 3.1 in chapter 3.3) accordingly. In most cases, the variations were lower than variations of the oxide film thickness throughout the same Ni wafer.

A.3. Results and Discussion

Figure A.1. compares the dielectric function of Ni as recommended in the literature [8] to data of a Ni wafer covered by its room temperature oxide layer as measured with the spectroellipsometer used in this study. It is seen that deviations from the recommended literature values for the dielectric constants are at all energies less than $\Delta e = 2$, in line with an earlier conclusion [32,33] that the small amounts of NiO present on Ni at room temperature (typically quoted figures are 50 Å [34]) do not influence the measured optical properties in a very pronounced manner. However, it has proved impossible to analyse the measured pseudodielectric function in terms of a single-oscillator overlayer model assuming the presence of NiO, as the parameters obtained for any good fit are always physically nonsensical. This could be taken as an indication that the origin of the deviations from the literature values is actually not

the native NiO overlayer but surface roughness and/or crystal lattice distortions due to diamond polishing. However, a surface roughness analysis based on the assumption of a surface layer consisting of voids and Ni likewise did not lead to agreement with the recommended literature data. This leaves only experimental errors and errors in the literature values as possible origins of the small disagreement between the datasets. It should be noted that the recommended literature values [8] were obtained using a different experimental approach, namely a Kramers-Krönig analysis and extrapolation into the visible light range of infrared absorptivity data [32]. Some deviations between datasets due to technical differences are therefore expected. In line with this, it has previously been suggested that the spectroellipsometrically determined dielectric function of Ni might deviate from the recommended values [33]. Especially at energies over 4 eV, experimental values should be interpreted bearing in mind that the intensity of the Xe light source, and therefore the accuracy of the measurement, deteriorates somewhat. Mainly for reasons of consistency, the present data analysis was carried out using the ellipsometrically determined dielectric function of the Ni substrate rather than the literature values.

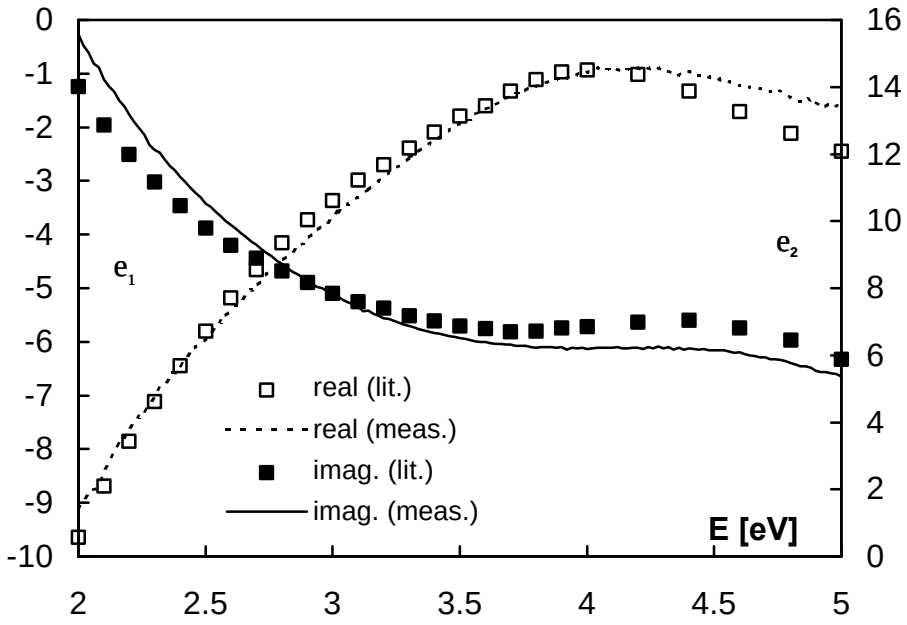

Figure A.1. Real (ε_1) and imaginary (ε_2) parts of the complex dielectric function of metallic Ni as reported in the literature (open and filled squares) and as measured in the present study using a diamond polished Ni wafer covered by its native room-temperature oxide layer. The error margin for literature- and experimental values is of the order of the second significant digit.

A representative example for the quality of the overlayer analysis is given in figure A.2, for the case of a Ni wafer covered by an overlayer of 1250 Å thickness. It is seen

that the measured pseudodielectric function of the sample is dominated by an absorption-like feature at approximately 2.35 eV which is due to interference between the light waves reflected at the overlayer/ambient- and substrate/overlayer-interfaces [35]. Such interference 'fringes' in the visible region have been observed for all samples with oxide overlayers over 200 Å. Their presence is in line with the observation that the oxidised Ni surfaces are characterised by very intense colours. Having interference features in the spectra is also fortunate for the fitting analysis of the data because the energetic position of the fringes is a strong function of the overlayer thickness and less so of other parameters in the signal oscillator model dielectric function. This strong correlation ensures accurate results in the thickness determination. In line with this, it was found that the overlayer thicknesses obtained from the data fitting analysis were quite insensitive (less than ±5%) to the actual choice of the parameters in the model dielectric function. The same observation has been made previously in the analysis of well-defined ZnS films [6].

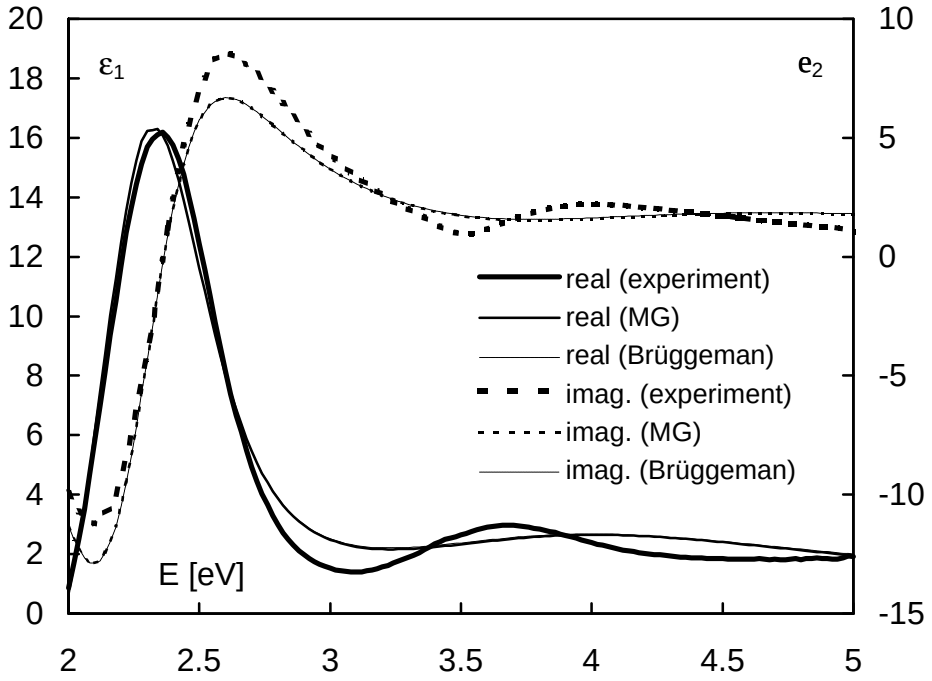

Figure A.2. Real (e_1, full thick line) and imaginary (e_2, broken thick line) parts of the complex dielectric function measured on a Ni wafer covered by 1250 Å (±20%) of NiO. Note the strong 'absorption' band at 2.35 eV due to interference between the light reflected from the air/NiO and NiO/Ni interfaces (see text).

An estimate for the variation of the overlayer thickness within a single Ni wafer was obtained by recording ellipsometric spectra at several spots on the wafer surface (at the front, the middle and the end). Figures A.3, A.4 and A.5 display the model parameters obtained from the analyses as a function of oxide overlayer thickness. Pronounced trends are seen mainly in the low overlayer thickness regime (below

500 Å): here, the static and high-frequency dielectric constants (fig. A.3) increase somewhat as a function of overlayer thickness until they approach the vicinity of their bulk value (11.8 ± 0.5 and 5.4, respectively [36]) at high film thicknesses. Correlated with these increases, the frequencies of the transversal lattice vibrations w_0 and the damping term g decrease as a function of oxide thickness (fig. A.4). It appears unlikely that these variations are physically significant, as they are less pronounced when the damping frequency is deliberately set to zero (which is equivalent to employing the undamped single oscillator model given by equation (A.11)). A negligibly small damping frequency would indicate the formation of a non-absorbing, and therefore defect-free overlayer - characteristics, which would be in line with the known tendency of Ni to form initially transparent, epitaxial NiO overlayers free from lattice strain [34,37]. Inspection of equations (A.13a) and (A.13b) adds further evidence of the artificial origin of the trends seen at low overlayer thicknesses: a strong correlation between the dielectric constants and the damping factor should exist because a large value for g does always results in a decrease of the complex dielectric constants e_1 and e_2. This decrease can be offset by larger values for the model dielectric constants e_0 and e_∞. In line with this, it was observed that the fit quality as well as the best-fit thickness and effective medium parameters were insignificantly changed by the suppression of the damping term in the low thickness region.

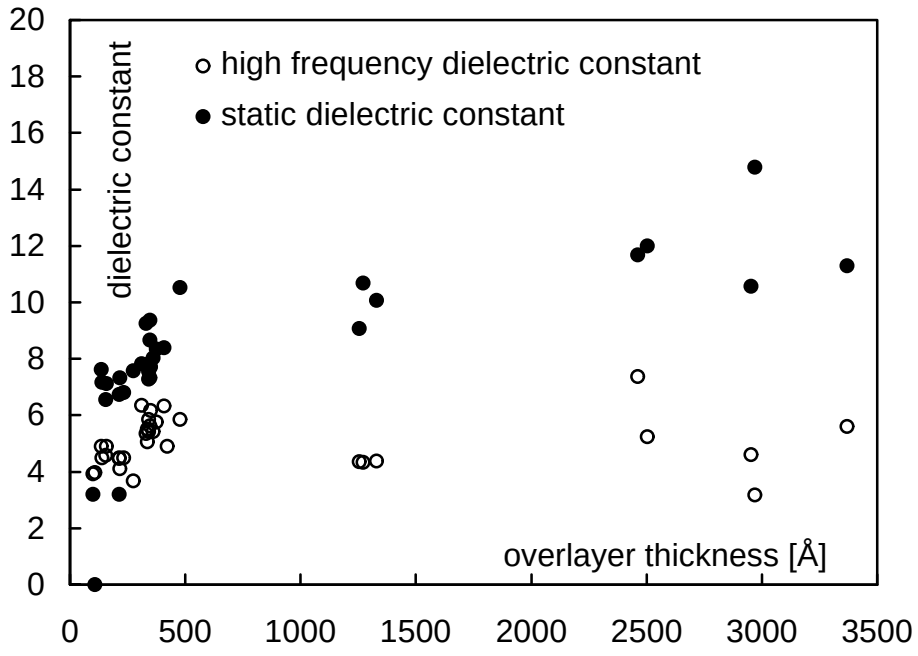

Figure A.3. Overlayer thickness dependence of the model dielectric constants as derived within the damped single oscillator approximation.

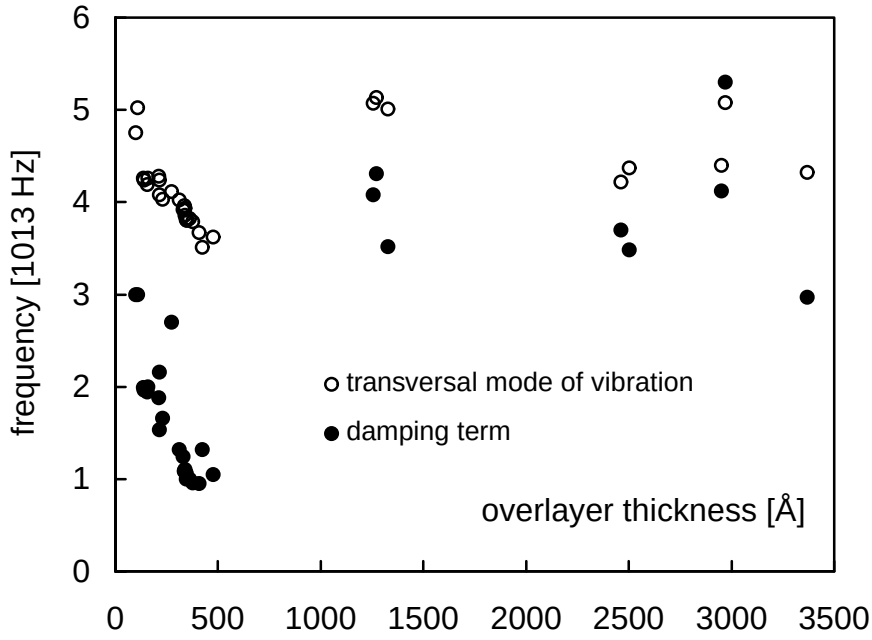

Figure A.4. Frequency of the transversal vibration mode (w_0) and the damping term γ in the fitted single oscillator model. See text for discussion of trends.

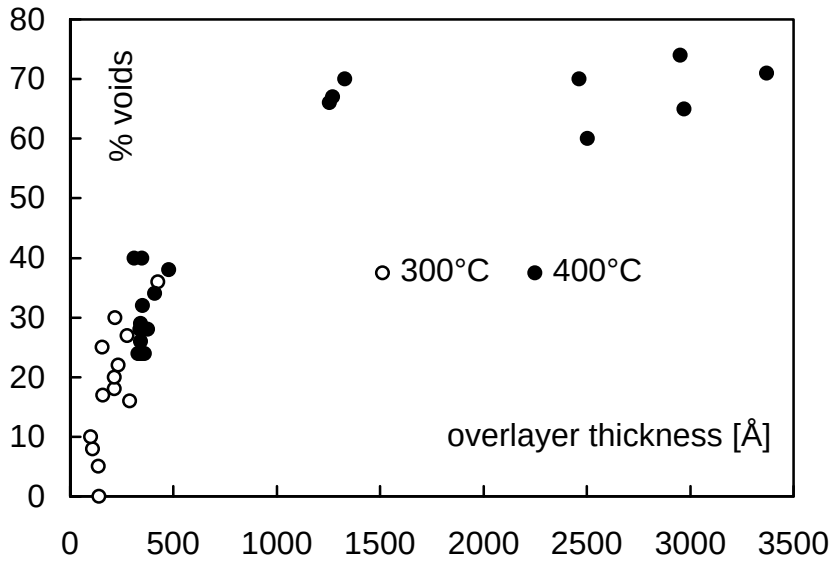

Figure A.5. Void fraction in the NiO overlayer (determined with the Maxwell-Garnett effective medium approximation) as a function of film thickness.

Long exposure of Ni to oxygen is known to result in the growth of increasingly defective NiO overlayers [37]. These are expected to exhibit light absorbing properties (NiO prepared at low temperatures usually appears black, while stoichiometric NiO is light green), and indeed, the ellipsometric analysis reflects this tendency to non-stoichiometry as a strong increase of the damping term at higher

overlayer thicknesses (fig. A.4). Obviously, broad-band absorption of light in the defective lattice and scattering decrease the sample reflectivity.

Strong heterogeneity of the thicker overlayers is borne out by the volume fraction of voids derived from the MG effective medium fit to the data (fig. A.5). The analysis yielded void fractions of 60% - 70% for the highest overlayer thicknesses. On first sight, these values might appear high, but it must be remembered that the oxide growth on Ni proceeds in a very inhomogenous manner after a smooth passivating layer has been formed. The NiO crystallites are formed preferentially in the vicinity of grain boundaries and cracks in the overlayer. Lattice diffusion of Ni^{2+} limits the oxidation only at temperatures over 800°C-900°C, and even then only after the formation of very thick scales of typically some 15 μm [37]). The formation of irregular crystallite shapes at oxide thicknesses over a few 100 Å is well documented, and leads to rough and heterogeneous oxide scales [37,38]. At lower overlayer thicknesses, the NiO overlayers are much more compact as a result of the small lattice misfit between NiO and Ni which enables the homogeneous growth of epitaxially oriented crystallites. It is known from single crystal studies that a high degree of epitaxial orientation of the NiO overlayer can be maintained even at thicknesses in the vicinity of 350 Å [37]. The small void fractions determined from the spectroellipsometric data at low overlayer thicknesses are therefore confirming well-established expectations. Scanning electron microscopy and X-ray diffraction have shown that the subsequent scale growth on polycrystalline Ni proceeds at these thicknesses predominantly by increasing the number of small oxide crystallites [37]. When the scale thickness approaches 1000 Å, recrystallisation and grain growth/fusion take over as the dominant mechanism. The morphology of the scale formed in this last growth regime is strongly dependent on its starting morphology, which is, in the case of a polycrystalline sample, characterised by a comparatively high number of grain boundaries. As a result, very inhomogeneous scale growth follows. Dendritic, columnar grains with substantial voids between them are usually visible in electron micrographs of thick NiO scales [37,38]. The ellipsometrically determined void fractions for the thickest scales are therefore expected to be high. Note in this context that void fractions as high as 80% have previously been observed for other oxide overlayers [39], as well as for Si films grown on GaAs [22]. Figures in the range between 20% and 50% are commonplace even for materials grown under controlled conditions [11,29,40].

Finally, figure A.6. illustrates that the oxide thicknesses, obtained by taking account of the void fractions, agree very well with gravimetrically obtained values [41] for the same temperature range. The original gravimetric data have been converted into oxide thicknesses by assuming that the overlayer is void-free and characterised by the

bulk density (6.67 g/cm3) of NiO. Note that the reproduced dataset of Uhlig *et al.* [41] was obtained at an oxygen pressure of 1 atm, while the present NiO films were grown at 0.2 atm. However, the pressure difference is not expected to have a substantial influence on the results because the oxide growth rate is only a weak function ($p_{O_2}^{1/6}$) of the partial oxygen pressure [38]. Moreover, the rate of Ni oxidation is well known to be strongly dependent on experimental conditions, such as sample history, purity, residual hydrogen content of the Ni lattice, surface roughness etc. Rate variations of ±50% between sample runs are common (compare data given in [37,41,42]). The impact of varying the oxygen pressure between 0.2 atm and 1 atm is therefore negligible compared to the error margins of the experimental oxidation rates. Note, however, that the present data exhibit the typical two-stage logarithmic growth law which has previously been observed in several studies [37,41,42].

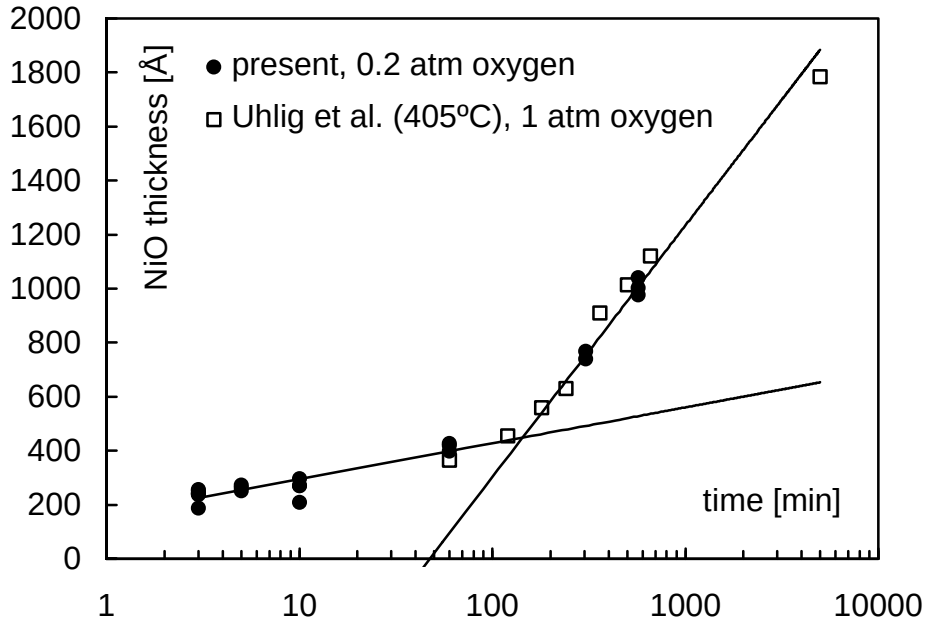

Figure A.6. Oxide overlayer thickness as a function of oxidation time for at temperatures in the vicinity of 400°C (± 10°C). A dataset taken from the work of Uhlig *et al.* [41] (open squares) has been plotted for comparison with the present results (filled circles). The figure illustrates that the oxide thicknesses determined in the present study are in good agreement with gravimetrically obtained values. Note in particular that the previously observed 'two-stage logarithmic' growth law, here indicated by the lines which were least-squares fitted to the present data, is very well reproduced.

A.4. References

[1] B. Drevillon, J. Perrin, R. Marbot, A. Violet, J.L. Darby, Rev. Sci. Instrum. 53 (1982) 969.

[2] G. Jungk, Thin Solid Films 234 (1993) 428.

[3] S.N. Jasperson, S.E. Schnatterly, Rev. Sci. Instrum. 40 (1969) 761.

[4] R.M.A. Azzam, N.M. Bashara, *Ellipsometry and Polarized Light* (North-Holland, Amsterdam, Oxford, 1977).

[5] G.R. Boyer, B.F. Lamouroux, B.S. Prade, Appl. Opt. 18 (1979) 1217.

[6] G.E. Jellison Jr., J.W. McCamy, Appl. Phys. Lett. 61 (1992) 512.

[7] G.E. Jellison Jr. Thin Solid Films 234 (1993) 416.

[8] *Handbook of Optical Constants of Solids* (Academic Press, Orlando, 1985).

[9] S.Y. Kim, K. Vedam, Thin Solid Films 166 (1988) 325.

[10] K. Vedam, S.Y. Kim, Appl. Opt. 28 (1989) 2691.

[11] G.E. Jellison Jr. J. Appl. Phys. 69 (1991) 7627.

[12] C. Kittel, *Introduction to Solid State Physics* (Wiley, New York, 1986).

[13] D.M. Adams, *Vibrational Spectroscopy,* in: Solid State Chemistry. Techniques, ed. by A.K. Cheetham and P. Day (Clarendon Press, Oxford, 1987) 322.

[14] M. Born, K. Huang, *Dynamical Theory of Crystal Lattices* (Clarendon Press, Oxford, 1954).

[15] K. Huang, Proc. Roy. Soc. Lond. A 209 (1951) 352.

[16] J.C. Maxwell Garnett, Phil. Trans. R. Soc. London 203 (1904) 385.

[17] J.C. Maxwell Garnett, Phil. Trans. R. Soc. London A205 (1906) 237.

[18] R.W. Cohen, G.D. Cody, M.D. Coutts, B. Abeles, Phys. Rev. B 8 (1973) 3689.

[19] L.D. Landau, E.M. Lifshitz, *Electrodynamics of Continuous Media* (Addison-Wesley, Reading, Mass. 1960).

[20] F.L. Galeener, Phys. Rev. Lett. 27 (1971) 421.

[21] F.L. Galeener, Phys. Rev. Lett. 27 (1971) 1716.

[22] D.E. Aspnes, J.B. Theeten, F. Hottier, Phys. Rev. B 20 (1979) 3292.

[23] D.E. Aspnes, *The Accurate Determination of Optical Properties by Ellipsometry,* in: Handbook of Optical Constants I, ed. by E.D. Palik (Academic Press, Orlando, 1985) 89.

[24] G.A. Niklasson, C.G. Granqvist, O. Hunderi, Appl. Opt. 20 (1981) 26.

[25] D.A.G. Brüggeman, Ann. Phys. 24 (1935) 637.

[26] D. König, W.H. Weber, B.D. Poindexter, J.R. McBride, G.W. Graham, K. Otto, Catal. Lett. 29 (1994) 329.

[27] G. Parjadis de Larivière, M. Frigerio, F. Bridou, J. Rivory, Thin Solid Films 234 (1993) 458.

[28] K. Vedam, P.J. McMarr, J. Narayan, Appl. Phys. Lett. 47 (1985) 339.

[29] P.J. McMarr, J.R. Blanco, K. Vedam, R. Messier, L. Pilione, Appl. Phys. Lett. 49 (1986) 328.

[30] Z. Hashin, S. Shtrikman, J. Appl. Phys. 33 (1962) 3125.

[31] C.G. Granqvist, O. Hunderi, Phys. Rev. B 16 (1977) 3513.

[32] D.W. Lynch, R. Rosei, J.H. Weaver, Solid State Commun. 9 (1971) 2195.

[33] B.Y. Yang, B. Klosowski, K. Vedam, J.S. Lannin, Phys. Rev. B 38 (1988) 1562.

[34] C.R. Brundle, J.Q. Broughton, *The initial interaction of oxygen with well-defined transition metal surfaces,* in: The Chemical Physics of Solid Surfaces and Heterogeneous Catalysis Vol.3: Chemisorption Systems, Part A, ed. by D.A. King and D.P. Woodruff (Elsevier, Amsterdam, Oxford, New York, Tokyo, 1990) 131.

[35] M. Born, *Optik. Ein Lehrbuch der elektromagnetischen Lichttheorie* (Springer, Berlin, 1933).

[36] R. Newman, R.M. Chrenko, Phys. Rev. 114 (1959) 1507.

[37] W.W. Smeltzer, D.J. Young, Progress in Solid State Chemistry 10 (1975) 17.

[38] O. Kubaschewski, B.E. Hopkins, *Oxidation of Metals and Alloys* (Butterworths, London, 1967).

[39] J.S. Brodkin, L.C. Sengupta, W. Franzen, P.L. Sagalyn, Thin Solid Films 234 (1993) 512.

[40] P. Chindaudom, K. Vedam, Thin Solid Films 234 (1993) 439.

[41] H. Uhlig, J. Pickett, J. MacNairn, Acta Met. 7 (1959) 111.

[42] H.-J. Engell, K. Hauffe, B. Ilschner, Z. Elektrochem. 58 (1954) 478.